Journal Pre-proofs

Manganese catalyzed transfer hydrogenation of biomass-derived aldehydes: insights to the catalytic performance and mechanism

Yunchao Feng, Sishi Long, Guihua Yan, Binglin Chen, Jonathan Sperry, Wanjie Xu, Yong Sun, Xing Tang, Xianhai Zeng, Lu Lin

PII: S0021-9517(20)30218-9
DOI: https://doi.org/10.1016/j.jcat.2020.05.037
Reference: YJCAT 13767

To appear in: *Journal of Catalysis*

Received Date: 12 May 2020
Accepted Date: 25 May 2020

Please cite this article as: Y. Feng, S. Long, G. Yan, B. Chen, J. Sperry, W. Xu, Y. Sun, X. Tang, X. Zeng, L. Lin, Manganese catalyzed transfer hydrogenation of biomass-derived aldehydes: insights to the catalytic performance and mechanism, *Journal of Catalysis* (2020), doi: https://doi.org/10.1016/j.jcat.2020.05.037

This is a PDF file of an article that has undergone enhancements after acceptance, such as the addition of a cover page and metadata, and formatting for readability, but it is not yet the definitive version of record. This version will undergo additional copyediting, typesetting and review before it is published in its final form, but we are providing this version to give early visibility of the article. Please note that, during the production process, errors may be discovered which could affect the content, and all legal disclaimers that apply to the journal pertain.

© 2020 Published by Elsevier Inc.

Manganese catalyzed transfer hydrogenation of biomass-derived aldehydes: insights to the catalytic performance and mechanism

Yunchao Feng [a], Sishi Long [a], Guihua Yan [a], Binglin Chen [a], Jonathan Sperry [d], Wanjie Xu [e], Yong Sun [abc], Xing Tang [abc], Xianhai Zeng*[abc] and Lu Lin [abc]

[a] College of Energy, Xiamen University, Xiamen 361102, China.

[b] Fujian Engineering and Research Center of Clean and High-valued Technologies for Biomass, Xiamen 361102, China.

[c] Xiamen Key Laboratory of Clean and High-valued Utilization for Biomass, Xiamen 361102, China.

[d] Centre for Green Chemical Science, University of Auckland, Auckland 1142, New Zealand

[e] College of Materials, Xiamen University, Xiamen 361102, China.

KEYWORDS

biomass conversion, 5-hydroxymethylfurfural, transfer hydrogenation, manganese hydrogenation catalysis; mechanism study

Corresponding Author

*E-mail: xianhai.zeng@xmu.edu.cn (Xianhai Zeng)

Journal Pre-proofs

Abstract

Manganese catalyzed transfer hydrogenation (CTH) of aldehydes is an attractive method for the synthesis of alcohols. Here, we report a novel and efficient MnO@C-N catalyst for the CTH of biomass-derived 5-hydroxymethylfurfural and other aldehydes to alcohols in high yields. Catalytic experimental studies showed that the MnO and nitrogen-doping are responsible for the high selectivity and high conversion, respectively. Isotopic labelling experiments demonstrated that the CTH of aldehydes to alcohols over MnO@C-N is via a route by direct hydrogen transfer. Kinetic studies revealed that the N-doping can improve the reaction rate and reduce the activation energy of the aldehydes conversion. DFT calculations also indicated that both pyridine N and pyrrolic N doping can reduce the energy barrier for acetone desorption by the interaction between N and hydroxyl-H of alcohol. Furthermore, MnO@C-N showed good recyclability for at least five reaction cycles. We anticipate that these results can drive progress in the manganese catalyzed transfer hydrogenation reaction.

1. Introduction

Emerging energy crises and environmental problems have promoted worldwide attention to develop sustainable biomass resources to the diminishing fossil fuels[1-3]. 5-hydroxymethylfurfural (HMF) is widely considered as an important platform intermediate for transforming lignocellulosic biomass into high-value-added chemicals and biofuels[4-6]. Particularly, selective hydrogenation of HMF to 2, 5-dihydroxymethylfuran (DHMF) has potential industrial applications in the synthesis of resins, foams, polymers, drugs, artificial fibers and biodiesel[7-10].

To date, considerable catalytic systems for the selective hydrogenation of HMF are focused on transition metals (e.g., Ru[11, 12], Pt[13-15], Pd[16, 17], Ir[18], Ni[11], Cu[19, 20], Co[21, 22])

using H_2 as the hydrogen source. Compared to the H_2-hydrogenation reaction, catalytic transfer hydrogenation (CTH) represents an attractive, safer and more convenient alternative for the hydrogenation of aldehydes, especially targeting large-scale applications. For example, no autoclaves and external H_2 are required using alcohols as both solvent and hydrogen donors. So far, various precious metal catalysts (e.g., Au[23], Ru[24-27]) have shown excellent results for the CTH of biomass-derived aldehydes. However, the main drawback of these noble catalysts is its high cost. Meantime, relatively cheap rare metal catalysts (e.g., Hf[25, 26] and Zr[27-35]) have been developed as outstanding catalysts for the CTH of HMF and other aldehydes. Despite the great achievement, further developing inexpensive and widely abundant first-row base metals (such as Fe, Cu, Co, Mn) is expected[28]. Recently, unremitting efforts toward the design and synthesis of earth-abundant metal catalysts (e.g., Fe[29-31], Co[32-34], Cu[35, 36]) are going, which encourage us to explore a novel and effective base metal catalyst for CTH of aldehydes.

Manganese, as the third most abundant transition metal in the Earth's crust, is a potential candidate to replace rare or precious metals if comparable catalytic activities have resulted. Manganese catalyzed transfer hydrogenation of aldehydes is introduced by the Beller's group in 2016 using manganese pincer complexes[37]. Further seminal work was published by the groups of Sortais using commercially available and cheap 2-picolylamine as a ligand[38]. Later, Qi group reported a manganese-based carbon aerogel for the CTH of HMF[39]. However, despite these achievements, homogeneous Mn catalysts resulted in recycled issues[37, 38], strong base employment [37-39] and low selectivity[39] are remained in this manganese catalyzed CTH reaction. Thus, to develop highly selective Mn-based catalysts with base free and further understand the reaction mechanism is highly desired to Mn catalyzed transfer hydrogenation of aldehydes.

Journal Pre-proofs

In this work, we demonstrate that N-doped carbon supporting MnO nanoparticles (MnO@C-N) are highly active and selective for the CTH of biomass-derived HMF and other aldehydes to alcohols with base free. The catalyst fabrication process is simple and sustainable. Furthermore, the catalyst characterization and catalytic performance were investigated in detail, and the reaction mechanism was further revealed by deuterium isotope tracing experiments and DFT calculations. To the best of our knowledge, there have been no previous reports on the use of MnO based catalysts for transfer hydrogenation reaction. We anticipate that these results can drive progress in the Manganese catalyzed transfer hydrogenation reaction.

2 Experimental section

2.1 Materials

All reagents were supplied by Aladdin Chemical Technology Co. Ltd. (Shanghai, China) and used without further purification.

2.2 Synthesis of MnO@C-N

In a typical synthesis, Manganese(Ⅱ)acetate tetrahydrate, sucrose and urea in a mass ratio of 1:1:10 were dissolved in a 300mL 70% ethanol solution. The solution was distilled in 85 ^{o}C until the solvent was completely removed. The as-obtained sol-gel mixture was dried at 100 ^{o}C for 5h. Subsequently, the mixture was placed in a tube furnace and heated to 300 ^{o}C for 1h, and then pyrolyzed at 700 °C for 2h with a heating rate of 5 ºC/min under N_2 atmosphere.

2.3 Synthesis of MnO@C

In a typical synthesis, 1g manganese carbonate powder was mixed with sucrose (2.5 g, 5g, 10g or 15g) for MnO@C (20 nm), MnO@C (15 nm), MnO@C (8 nm) or MnO@C (5 nm) respectively. The resulting solid powder was heated at 600 °C for 2h under an N_2 atmosphere.

2.4 Catalyst characterization

Powder X-ray diffraction patterns of the samples were recorded on a Rigaku D/max X-ray diffractometer using Cu Kα radiation (40 kV, 30 mA, λ = 0.1543 nm). Raman spectra were measured on a Renishaw inVia Raman microscope with 633 nm laser excitation. The laser power was 10 mW, and the spot size was 2 m. BET surface areas and pore sizes measurements were performed with N_2 adsorption/desorption isotherms using a TriStar 3000 with the BET and BJH methods. CO_2/NH_3 temperature-programmed desorption (CO_2/NH_3-TPD) was measured on a Micromeritics AutoChem II 2920, equipped with a thermal conductivity detector (TCD). Metal contents of the samples were determined using Inductively Coupled Plasma Optic Emission Spectrometer (ICP-OES, Varian (720)). The size and morphology of materials were studied by scanning electron microscopy (SEM, SUPRA 55) high-resolution transmission electron microscopy (HR-TEM, JEM-2100). The X-ray photoelectron spectroscopy (XPS) measurements were performed on a Thermo ESCALAB 250XI electron spectrometer with a monochromatic Al Kα radiation (hv=1486.8 eV) and the spot size of all spectra was 650μm. NMR studies were tested by Agilent 400M.

2.5 Simulation methods

We used a 5×6 supercell graphite (001) to simulate the graphite monolayer. One C atom was deleted and another one was replaced by N atoms in the graphite(001) monolayer to simulate graphite-pyridinic-N monolayer. To simulate the MnODots-granite-pyridinic-N composites, MnODots($Mn_{14}O_{14}$) were stacked on the granite-pyridinic-N surface slab. The height of the supercell is set as 20A˚ to ensure negligible interaction between adjacent slabs. In this work, the density functional theory (DFT) calculation was performed by the Cambridge serial total energy package (CASTEP)[40] code, in which a plane wave basis set was used. The exchange and correlation interactions were modeled using the generalized gradient approximation (GGA) and

the Perdew-Burke-Ernzerhof (PBE)[41] functional. Grimme's semi-empirical DFT-D[42] was introduced in the computations to guarantee a better description of the electron interaction in a long-range. The Vanderbilt ultrasoft pseudopotential[43] was used with a cutoff energy of 370 eV. Geometric convergence tolerances were set for the maximum force of 0.03 eV/A˚, maximum energy change of 10^{-5} eV/atom, the maximum displacement of 0.001 A˚ and maximum stress of 0.5 GPa. Density mixing electronic minimisation was implemented and the self-consistent field (SCF) tolerance was set to ''fine'' with high accuracy of 10^{-6} eV/atom for energy convergence.

Other simulation was studied as the identical method as MnO@C-N (pyridinic N).

2.6 CTH of HMF

In a typical run， 0.26g of HMF, 0.1g of catalyst and 20mL of isopropanol were added in a stainless steel reactor equipped with a magnetic stirrer and heated to target temperature within 50 min. The reaction time was started to record as soon as the system reached working temperature. After completion of the reaction, the catalyst was separated and a sample of the liquid mixture was subjected to GC analysis. The conversion of 5-HMF and the yield of products were calculated according to the following equations:

$$\text{HMF conversion} = \left(1 - \frac{\text{Moles of HMF}}{\text{Moles of HMF loaded}}\right) \times 100\%$$

$$\text{Product yield} = \left(1 - \frac{\text{Moles of product}}{\text{Moles of HMF converted}}\right) \times 100\%$$

3. Results and discussion

3.1 Catalyst preparation and characterization

To ensure the MnO@C-N materials could be suitable for large-scale production, the catalysts were prepared via direct carbonization (700°C, N_2) of a sol-gel mixture using cheap, available and sustainable sucrose, urea and manganese acetate as precursors as illustrated in Figure 1a.

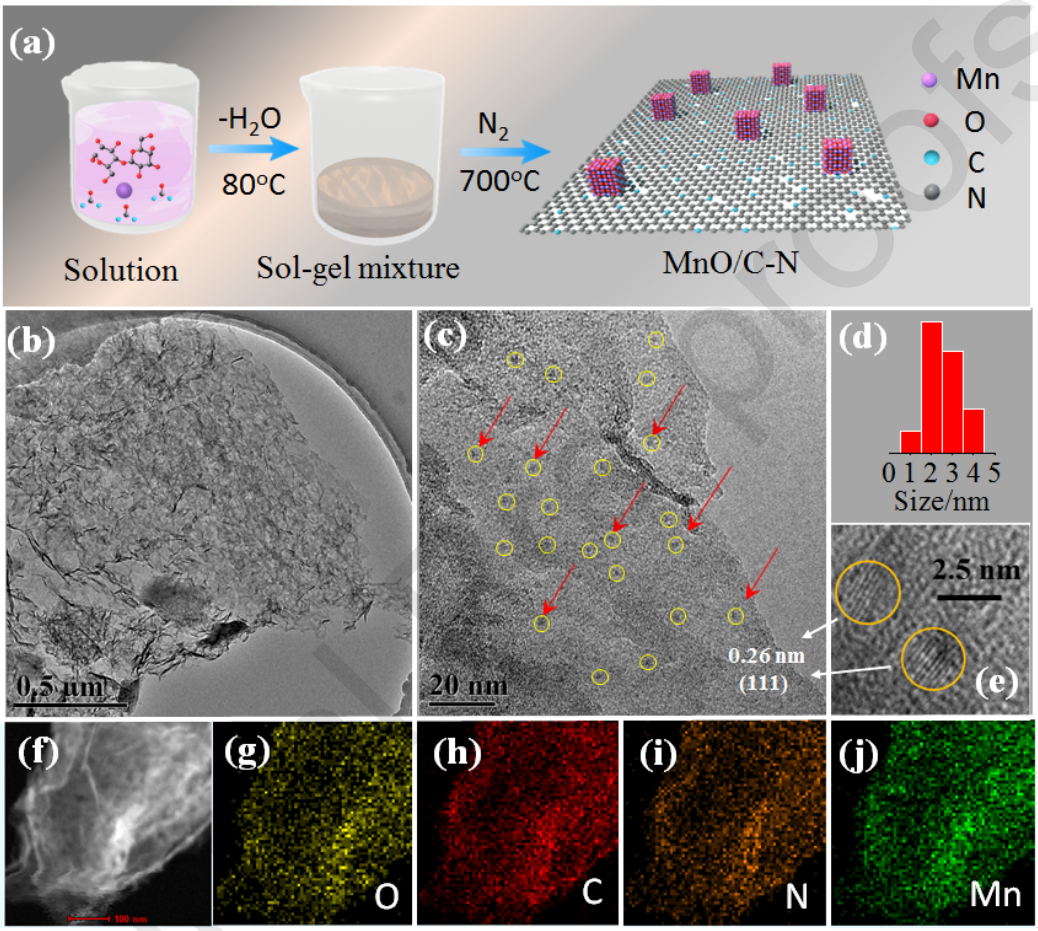

Figure 1. (a) Schematic illustration of the synthesis of MnO@C-N. (b-c) TEM images of MnO@C-N; part of MnO NPs are marked by red arrows. (d) The size distribution of MnO. (e) interplanar spacing of MnO (f-j) STEM image and the corresponding mapping of O, C, N and Mn for the catalyst MnO@C-N.

The morphology and microstructure were investigated by scanning electron microscopy (SEM) and transmission electron microscopy (TEM). As observed in Figure S1a (Supporting Information), MnO@C-N (700) shows a clear two-dimensional (2D) sheet structure, which is caused by the formation of the sacrificial template of graphitic carbon nitride (g-C_3N_4) when urea is heated over 550°C[44, 45]. Figure 1b and Figure S1b-f (Supporting Information) show no big nanoparticles. Figure 1c-1d reveal that ultrasmall MnO nanoparticles around 2–3 nm are homogeneously dispersed on C-N composites. Focusing on the enlarged view, clear crystalline interplanar spacings of MnO (111, 0.26 nm) can be observed (Figure 1e). Scanning transmission electron microscopy (STEM) image and its elemental mapping further confirm a highly uniform distribution of C, N, O and Mn on the surface of MnO@C–N materials (Figure 1f-j).

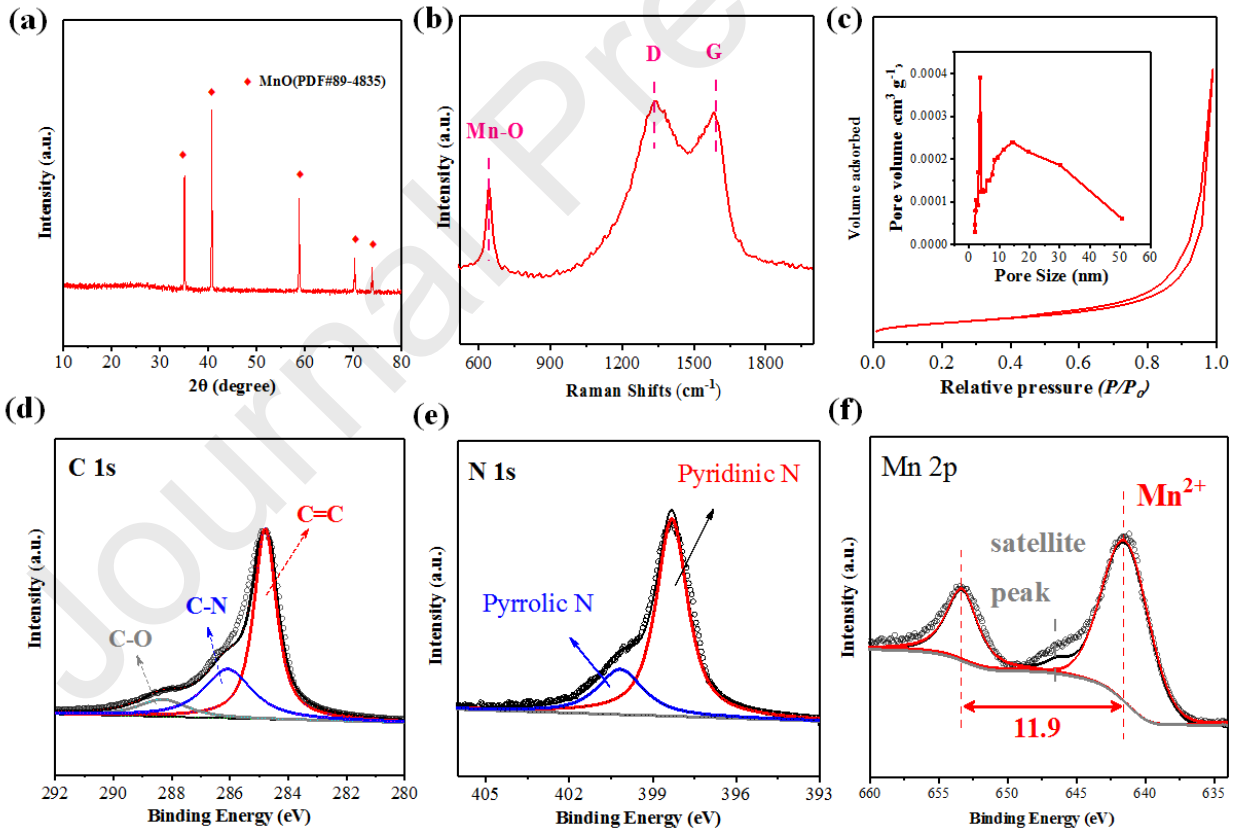

Figure 2. (a) XRD patterns, (b) Raman spectra, (c) BET analysis and pore-size distribution, (d) C 1s, (e) N 1s, (f) and Mn 2p of MnO@C-N.

The crystal structure and phase information of as-synthesized samples were confirmed by X-ray diffraction (XRD). As shown in figure 2a, the diffraction peak at around 35°, 41°, 59°, 70° and 73° can be attributed to cubic phase MnO (PDF#89-4835). While a diffraction hump between 22° and 28° corresponds to N-doped carbon (Figure S2, Supporting Information). Raman spectra were conducted to evaluate the graphitic quality of the carbon shells, as shown in figure 2b. There are two typical characteristic D band (~1350 cm^{-1}) and G bands (~1572 cm^{-1}), related to the disordered/defect carbon and graphitic sp^2-carbon, respectively[46, 47]. In addition, visible Mn-O vibrational bands at 647 cm^{-1} are also observed, suggesting the presence of manganese oxides[48, 49]. The pore-size distribution of as-prepared catalysts was also studied by N_2 adsorption-desorption analysis (Figure 2c). The specific surface area of MnO@C-N is 30.5 m^{2}g^{-1}. Additionally, the broad pore size distributions of 0 to 50 nm are obtained (inset in Figure 2c), revealing their micro- and mesoporous features. Both the appropriate specific surface area and porous characteristics are necessary for effective active sites accessibility and fast substrates and intermediates penetration.

The chemical composition and valence state were investigated by X-ray photoelectron spectroscopy (XPS). The XPS survey spectrum showed the presence of C, N, O, and Mn elements in MnO@C-N (Figure S3a, Supporting Information). The O 1s of three samples are shown in Figure S3b (Supporting Information), and Mn-O and C=O are observed at the peak of 531.2 and 529.8 eV, respectively[50, 51]. The high-resolution C 1s spectrum of MnO@C-N can be deconvolved into three bands, corresponding to C=C at ~284.8 eV, C-N at ~285.8 eV and C-O at ~288.7 eV (Figure 2d)[52, 53]. The N 1s peaks of all Mn@C-N materials show two deconvoluted

peaks at ~398.28eV and ~399.98 eV (Figure 2e), corresponding to pyridinic N and pyrrolic N, respectively[54]. The pyridinic-N replaces a carbon atom in C6 ring and bonds with two sp^2 carbon atoms; the pyrrolic N is in a five-membered ring and donates two electrons to the π system. It is well known that the pyridinic N and pyrrolic N, especially the pyridinic N can act as basic sites, which is beneficial to the proton transfer in CTH. In addition, the lone pair of electrons of N can change the local geometric and electronic structure of the carbon support, and thus preferentially nucleate the MnO NPs at N-occupied sites[55, 56]. The presence of several concentrated pyridinic N is the prominent peak in MnO@C-N. As shown in figure 2f, the high-resolution Mn 2p spectrum of MnO@C-N(700) exhibits two prominent bands at 641.5 eV ($2p^{1/2}$) and 653.4 eV ($2p^{3/2}$) with an energy difference of 11.9 eV, readily assigned to Mn^{2+}.[51] Meanwhile, a weak satellite peak is also presented at 646.5 eV (Figure 2f), which is another proof for the formation of MnO[51].

3.2 Catalytic performance of CTH of HMF to DHMF

To evaluate the catalytic activity of the as-synthesized MnO@C-N catalysts for the CTH of HMF, various alcohols are first investigated as H-donor/solvent (Figure 3a). Among the five applied alcohols, only isopropanol exhibits high reaction efficiency. These results indicate that the satisfying reactivity of MnO@C-N is largely dependent on the hydrogen donating ability of alcohols, which is secondary alcohol (isopropanol) > primary alcohol (methanol, ethanol, n-propanol and n-butanol). Figure 3b shows the influence of reaction temperature and time on the conversion of HMF to DHMF catalyzed by MnO@C-N. Generally, the DHMF yield increases with the increase of reaction time, and the HMF conversion is increased with temperature. A slight decrease of DHMF yield is observed when prolonging reaction time after 15h at 180 °C, owing to the over hydrogenation products such as 5-methylfurfural and 5-methylfurfuryl alcohol (detected

by GC-MS) are formed. Whilst, the maximum DHMF yield of 93% is achieved at 170°C with 21h. The reaction rates can be effectively improved by increasing catalyst concentration without significant drops in selectivity (Figure 3c, 3d). At the same time, a slight decrease in TOF value is observed with the increase of Mn dosages (Figure 3d).

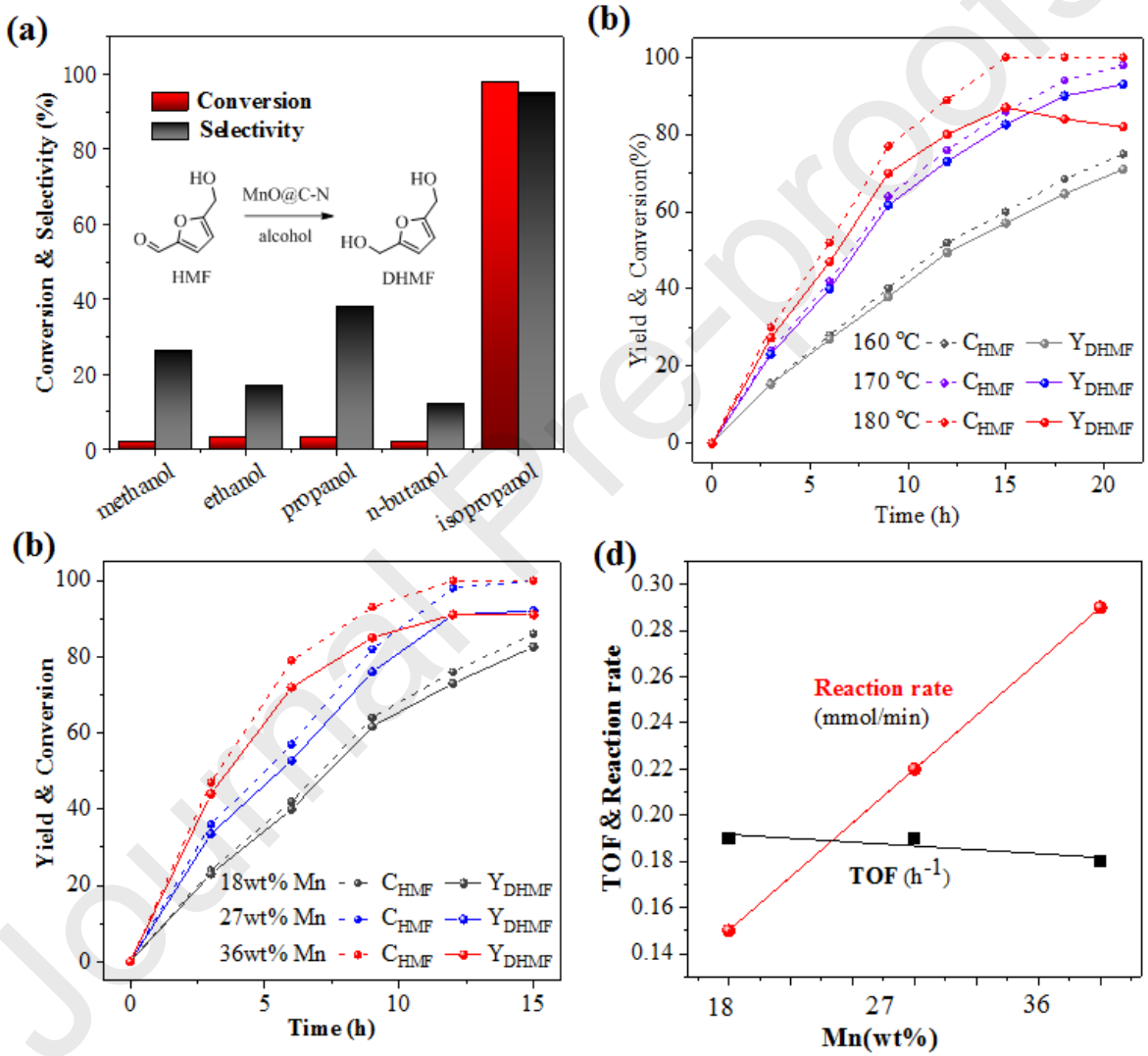

Figure 3. (a) CHT of HMF to DHMF by MnO@C-N using various alcohols, condition: 0.26g HMF, 0.1g catalyst, 20mL isopropanol, 170°C, 21h. C refers to conversion, while Y refers to yield.

(b, c) The effect of reaction temperature, reaction time, and dosage of catalyst on catalytic performance. (d) TOF values and reaction rate in various catalyst dosages.

3.3 Catalyst Recyclability

The heterogeneous nature of the MnO@C-N was checked by removing catalysts from the solution after 9 h of reaction, and heating the filtrate for another 12 h (Figure 4a). ICP-OES analysis of the reaction solution confirmed that the content of Mn was below the detection limit, suggesting no obvious Mn leaching during the reaction. The stability and recyclability of the MnO@C-N catalyst in the CTH of HMF to DHMF were further checked. As included in figure 4b, the catalyst could be reused at least five times without visible loss of activity or selectivity. XRD analyses and TEM images show that the crystal structure of MnO@C-N and highly dispersed MnO-NP remains almost the same before and after the reaction (Figure S4, S5, Supporting Information), confirming the excellent stability and recyclability of the material under the investigated conditions.

Journal Pre-proofs

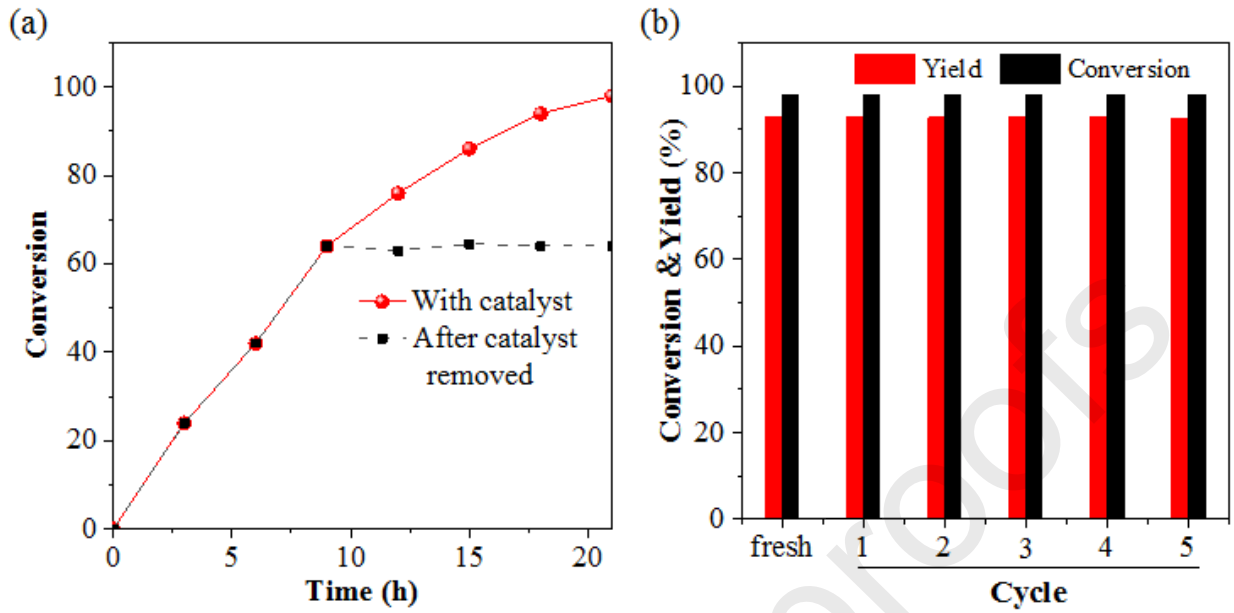

Figure 4. (a) leaching experiment of MnO@C-N; (b) Catalyst recycling studies for MnO@C-N. Condition: 0.26g HMF, 0.1g catalyst, 20mL isopropanol, 170°C, 21h.

3.4 CTH of other aldehydes

The excellent performance of the MnO@C-N catalyst was also investigated for the CTH of C=O bonds of a broad scope of substrates. As shown in Table 1, biomass-derived furanic aldehydes such as furfural and 5-methylfurfural, which are also important platform chemicals, are transformed smoothly into the corresponding alcohols with >95% selectivities at high conversions. With aromatic aldehydes and pyridine aldehydes as substrates, the desired products are also obtained in satisfying conversion and selectivity. Notably, the CTH of biomass -derivative ethyl levulinate can achieve 99% selectivity to γ-valerolactone. However, only 43% conversion of ethyl levulinate is obtained even at higher reaction temperature and prolonged duration, which can be attributed to the steric hindrance and electron-donating nature of the alkyl group in ketone.

Journal Pre-proofs

Table 1 CTH of various unsaturated aldehydes over MnO@C-N

Entry	Substrate	Product	Tep. (K)	Time (h)	Con. (%)	Sel. (%)
1			443	12	100	99
2			443	9	99	99
3			443	12	98	99
4			443	21	97	98
5			443	21	97	98
6			443	12	100	96
7			473	30	43	99

Condition: 0.26g HMF, 0.1g catalyst, 20 mL isopropanol.

3.5 Identifying the reaction mechanism

It was commonly known that three are two main mechanisms for the CTH reaction, namely, direct hydrogen transfer and metal-mediated hydrogenation. However, the mechanisms of manganese catalyzed transfer hydrogenation reaction is not clear up to now. In this case, mechanistic insight into the CTH of aldehydes to alcohols was investigated in 2-PrOH (d_8) by ex-situ NMR studies at various time. Furfural was chosen as a substrate due to its relatively simple structure, and the obtained ^{1}H NMR spectra were shown in Figure 5a. The proton of aldehyde (-CHO, 1a) groups are gradually disappeared with increasing the deuterium (D) addition from isotopic iPrOH-d8, accordingly resulting in the formation of methylene (-CH_2-, 1b) groups. However, the reaction mechanism between the direct hydrogen transfer and metal-mediated hydrogenation remains unclear by replacing 2-propanol-d_0 with 2-propanol-d_8. In order to differentiate these two possible pathways, t-butanol was introduced as co-solvent with 2-propanol-d8 because: (1) t-butanol cannot be used as a hydrogen donor due to the absence of β-H; and (2) it

is able to exchange D in the OD group of 2-propanol-d_8 or on the surface of the metal with H[27]. Accordingly, the desired alcohols should be produced with a 1 amu MS shift (MS+1) by direct hydrogen transfer (Figure 5b), or no mass shift (MS+0) by metal-mediated hydrogenation (Figure S6, Supporting Information). As expected, GC-MS analysis clearly shows a 1 amu mass shift of the parent ion (figure 5c), suggesting that the CTH of aldehydes to alcohols over MnO@C-N was via a route by direct hydrogen transfer.

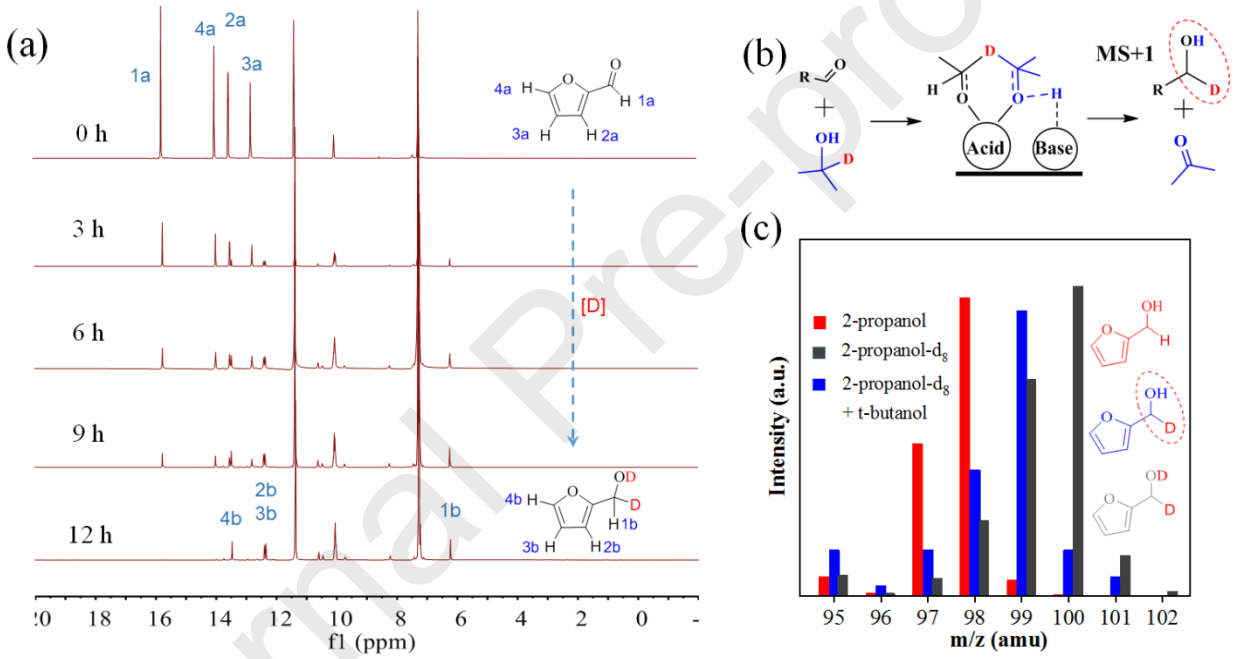

Figure 5. (a) Reaction kinetics study on CTH of furfural in isotopic iPrOH-d_8 using ^{1}H NMR. (b) mechanism of direct hydrogen transfer (c) Mass spectra of furfural alcohol.

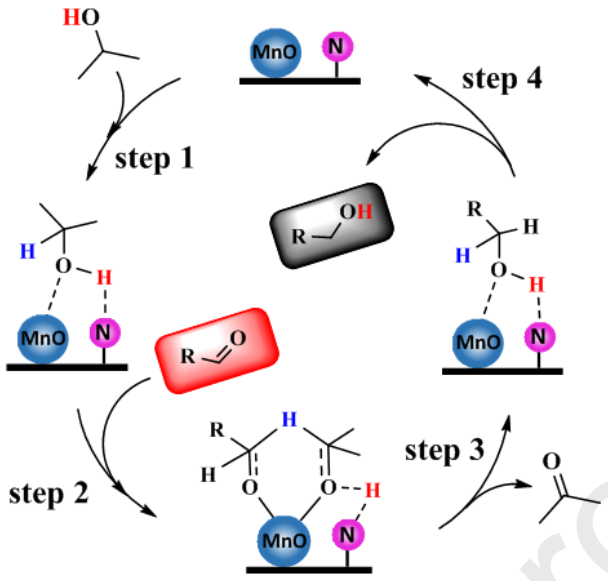

Figure 6. The proposed mechanism for CTH of aldehydes to the corresponding alcohols by MnO@C-N;

According to the above study, a typical direct hydrogen transfer mechanism was proposed in Figure 6a. Firstly, the aldehyde and alcohol groups are attracted by MnO NPs via the interaction between the lone pair electrons of oxygen and the strong electron-deficient MnO center to form a six-membered-ring intermediate. At the same time, the hydroxyl proton is extracted by N specials. Then, the α-H (blue H) is transferred from the α-C of the alcohol to the aldehyde carbon via a six-membered-ring intermediate, and hydroxyl-H is transferred to the aldehyde-O via an N-H intermediate.

3.6 Identifying the dominating factor for high selectivity and conversion

To figure out the key role of the various component in the MnO@C-N catalyst, various catalysts were first investigated for the CTH of HMF, as shown in Figure 7a. In the absence of any catalyst, almost no HMF conversion is observed. No DHMF selectivities are also observed when using

Journal Pre-proofs

activated carbon and C-N components (Figure S7, Supporting Information) as catalysts, while high selectivities up to 95% are achieved when MnO@C and MnO@C-N are applied. These controlled experiments demonstrated a crucial role of MnO for the high selectivity of DHMF.

Previous reports indicate that both nanoparticles' size and N-doping have a significant influence on catalytic activity[32, 57]. To check the effect MnO size and N-doping, a series of MnO with different size supported on carbon were first prepared (Figure S8, Supporting Information). As shown in figure 7b, The HMF conversion has a slight increase with the MnO size decreasing from 20 nm to 8 nm, while no obvious changes were observed when MnO size reduced to 5 nm. It can be expected that this conversion will not exceed 30%, even smaller size of MnO was used. However, with N-doping, high HMF conversion up to 98% is achieved, indicating that N-doping may play a dominating role for such high conversion.`

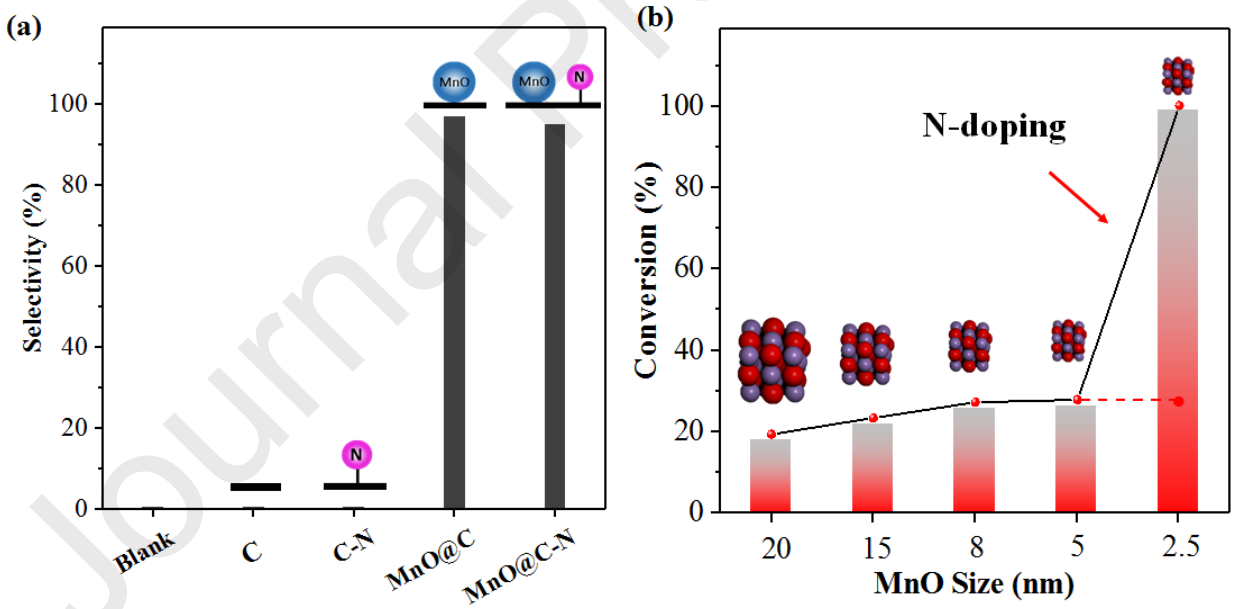

Figure 7. (a) CTH of HMF to DHMF by various catalysts; (b) the effect of MnO size on catalytic activity. Condition: 0.26g HMF, 0.1g catalyst, 20mL isopropanol, 170°C, 21h.

3.7 Revealing the key role of N-doping

The kinetic reaction, acid-base properties, and DFT calculation were studied to better understand the critical role of N-doping in the MnO@C-N catalyst. For comparison, the corresponding subjects for MnO@C with MnO size of 5nm (excluding the effect of MnO size) were also investigated. The time-dependent conversion catalyzed by MnO@C and MnO@C-N is shown in Figure 8a, MnO@C-N exhibits satisfying transformation and activity compared to MnO@C. Because of the high DHMF selectivity and ability in the investigated conditions, pseudo-first-order kinetics with respect to HMF can be used as the equation of $\ln c/c_0 = -kt$, where c is the concentration of HMF after a reaction time of t, c_0 is the initial concentration of HMF, and k is the rate constant. As shown in figure 8b, the plots of $\ln c/c_0$ versus t are satisfactorily linear, demonstrating the first-order reaction kinetics regarding the concentration of HMF. MnO@C-N displays a much higher rate constant (k) of 0.13 h^{-1}, 8.7-fold than that of MnO@C, 0.015h^{-1}. According to the Arrhenius equation of $\ln k = \ln A - E_a/RT$, the apparent activation energy (E_a) of the HMF conversion in the MnO@C-N(700)/isopropanol system is about 91 kJ/mol (Figure 8c), which is much lower than that of 131 kJ/mol for MnO@C catalyst. The result indicates that N doping can substantially improve catalytic efficiency.

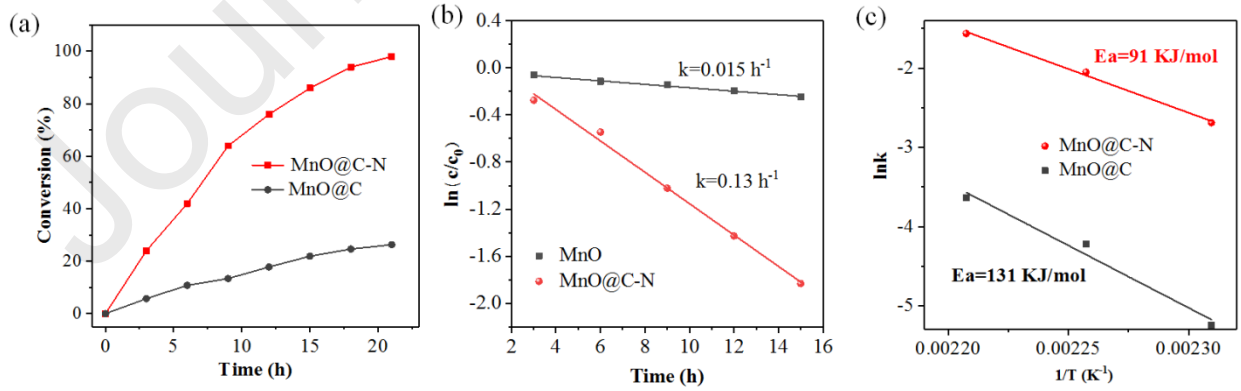

Figure 8. (a) The time-dependent conversion catalyzed by MnO@C and MnO@C-N, condition: 0.26g HMF, 0.1g catalyst, 20mL isopropanol, 170°C. (b) The kinetics profiles for the CHT of

HMF to DHMF (fitted by the first-order assumption). (c) Arrhenius plots for the CHT of HMF to DHMF.

According to the XPS N1s spectra analysis, N specials are mainly existing in the form of pyridinic N and pyrrolic N, which can provide basic sites or serve as electron donors due to its lone pair of electrons. Thus, the proton transfer processes are accelerated at N sites. The N-doping increase in basicity was also well demonstrated by the CO_2 temperature-programmed desorption (TPD) analysis (figure 9a). The MnO@C-N had a higher CO_2 desorption peak at ~ 280 °C and higher Lewis base strength and density than MnO@C (Figure 9c). In addition, it had been previously reported that N-doping carbon materials had a stronger electron coupling effect that facilitated electron transfer from metal/metal oxide NPs to N-doped carbon sheets[58-60], which can strengthen both basic and acidic sites. As expected, the acidity of MnO@C-N is clearly increased, as indicated by the stronger NH_3 desorption peaks (Figure 9b) and more acidic sites (Figure 9c) compared to MnO@C.

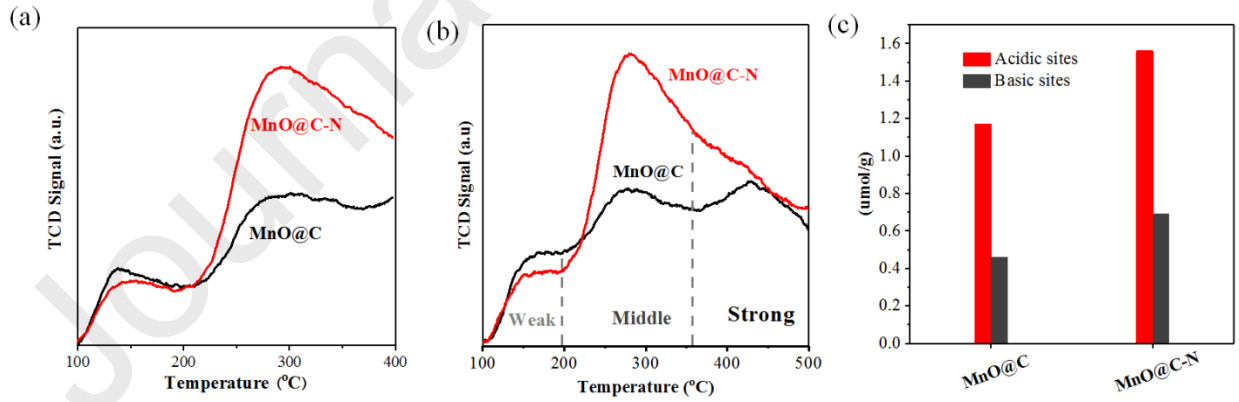

Figure 9. (a) NH_3-TPD and (b) CO_2-TPD spectrum. (c) Amount of acidic sites and basic sites

Based on the proposed reaction mechanism in Figure 6, density functional theory (DFT) calculation was performed to further understand how N-doping determines the activity of MnO for the CTH of HMF to DHMF (Figure 10a-c, Figure S9-S14). As shown in calculated energy profile and the transition state for the CTH on the active site (Figure 10b), the adsorption energy of isopropanol on MnO@C-N (Pyridinic N) is −1.67eV, lower than that of MnO@C (−1.52 eV) because of an effective N-H bonding interaction as indicated by the close N−H bond distance (2.6 Å). Both MnO@C and MnO@C-N (Pyridinic N) are able to absorb and stabilize isopropanol and HMF by forming a six-membered-ring intermediate (step 1 and step 2), and the reaction is drastically exothermic, with calculated reaction energy of -3.22 eV and -2.51 eV, respectively. The distance (2.2 Å) between hydroxyl-H (isopropanol) and N in MnO@C-N (Pyridinic N) is in the range of a typical hydrogen bond. The subsequent release of acetone and formation of DHMF on MnO@C is thermodynamically unfavorable by 1.85 eV and 1.34 (step 3 and step 4), respectively. As expected, the barrier in the presence of MnO@C-N (Pyridinic N) is notably reduced to 1.23 eV and 1.28 eV (step 3 and step 4), respectively, which can explain the experimentally observed high activity of MnO supported by pyridinic-nitrogen-doped carbon. Note that the pyridinic N-doping has a slight promoting effect on step 4, resulted by the weak interaction between N and hydroxyl-H of BHMF (4.3 Å). As shown in figure 10c, both of pyridinic N and pyrrolic N doping could reduce the energy barriers, especially for the step 3, and the lower barrier is obtained for MnO@C-N(pyridinic N), suggesting that N-doping improves the catalytic efficiency of CTH by reducing the energy barrier for acetone desorption.

Journal Pre-proofs

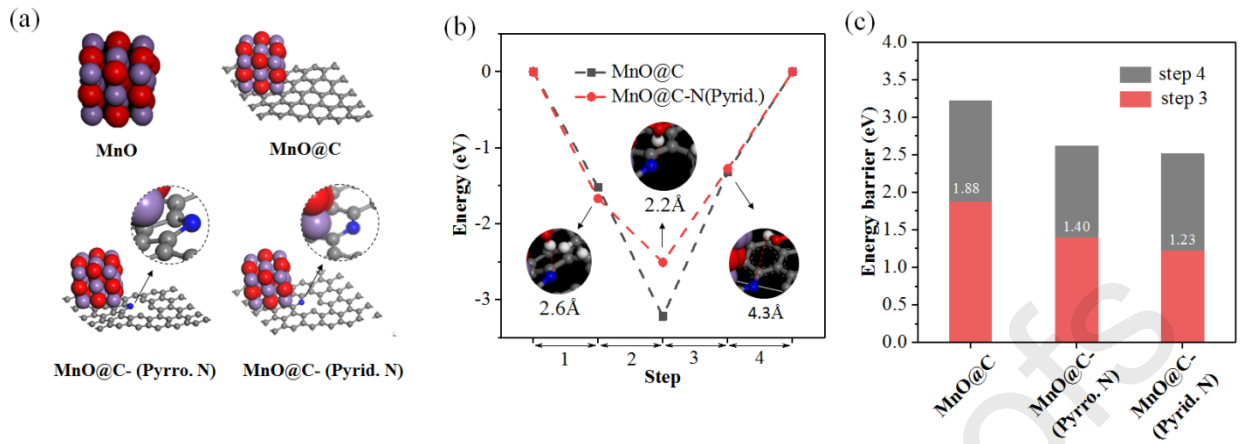

Figure 10. (a)Simulative atomistic structures of MnO, MnO@C, MnO@C-N(pyrrolic N), and MnO@C-N(pyridinic N). (e) Energy barriers of the CTH of HMF to DHMF by MnO@C, MnO@C-N(pyrrolic N), and MnO@C-N(pyridinic N).

4. Conclusion

In conclusion, cheap and sustainable MnO@C-N catalysts have been successfully prepared. Benefiting from the N-doping, ultrasmall MnO NPs with diameters of around 2.5 nm are generated and well dispersed on carbon supports. The as-prepared MnO@C-N catalysts show high selectivity and activity for the CTH of biomass-derived HMF and other aldehydes to the corresponding alcohols via direct hydrogen transfer. Compared to previous Mn-catalyzed CTH of aldehydes, the catalyst used in this work has advantages of higher selectivity and base-free. Experimental studies and DFT calculations demonstrate that the presence of MnO ensures the high selectivity of alcohols, and pyridine N-doping promotes the high conversion of aldehydes. Furthermore, the simple and scalable method for catalyst preparation and CTH reaction, giving a process that could be commercially viable.

Journal Pre-proofs

Acknowledgment

The authors gratefully acknowledge the financial support from the National Natural Science Foundation of China (No. 21978248), the Natural Science Foundation of Fujian Province of China (No.2019J06005). We also thank the New Zealand Ministry of Business, Innovation and Employment (MBIE) for support through the Catalyst Fund (16-UOA-049-CSG).

References

[1] E.L. Kunkes, D.A. Simonetti, R.M. West, J.C. Serrano-Ruiz, C.A. Gärtner, J.A. Dumesic, Science, 2008, 322, 417-421.
[2] S. De, J. Zhang, R. Luque, N. Yan, Energy & environmental science, 2016, 9, 3314-3347.
[3] Y. Feng, M. Li, Z. Gao, X. Zhang, X. Zeng, Y. Sun, X. Tang, T. Lei, L. Lin, J. Catal., 2019, 12, 495-502.
[4] R.-J. van Putten, J.C. Van Der Waal, E. De Jong, C.B. Rasrendra, H.J. Heeres, J.G. de Vries, Chem. Rev., 2013, 113, 1499-1597.
[5] L. Hu, L. Lin, Z. Wu, S.Y. Zhou, S.J. Liu, Renew. Sust. Energ. Rev., 2017, 74, 230-257.
[6] X. Kong, Y. Zhu, Z. Fang, J.A. Kozinski, I.S. Butler, L. Xu, H. Song, X. Wei, Green Chem., 2018, 20, 3657-3682.
[7] K. Weissermel, H.-J. Arpe, C.R. Lindley, S. Hawkins, Industrial organic chemistry, Wiley Online Library1997.
[8] X. Tang, J. Wei, N. Ding, Y. Sun, X. Zeng, L. Hu, S. Liu, T. Lei, L. Lin, Renewable Sustainable Energy Rev., 2017, 77, 287-296.
[9] J. Long, Y. Xu, W. Zhao, H. Li, S. Yang, Front. Chem., 2019, 7, 529.
[10] L. Hu, J. Xu, S. Zhou, A. He, X. Tang, L. Lin, J. Xu, Y. Zhao, ACS Catal., 2018, 8, 2959-2980.
[11] S. Yao, X. Wang, Y. Jiang, F. Wu, X. Chen, X. Mu, ACS Sustain. Chem. Eng., 2014, 2, 173-180.
[12] Z. Wei, J. Lou, C. Su, D. Guo, Y. Liu, S. Deng, ChemSusChem, 2017, 10, 1720-1732.
[13] G.-H. Wang, J. Hilgert, F.H. Richter, F. Wang, H.-J. Bongard, B. Spliethoff, C. Weidenthaler, F. Schüth, Nat. Mater., 2014, 13, 293-300.
[14] X. Wang, Y. He, Y. Liu, J. Park, X. Liang, J Catal, 2018, 366, 61-69.
[15] M. Chatterjee, T. Ishizaka, H. Kawanami, Green Chem., 2014, 16, 4734-4739.
[16] M. Audemar, K.D.O. Vigier, J.-M. Clacens, F. De Campo, F. Jérôme, Green Chem., 2014, 16, 4110-4114.
[17] P. Zhang, C.-H. Liu, L. Chen, J.-M. Chen, Y. Guan, P. Wu, J. Catal., 2017, 351, 10-18.
[18] M. Tamura, K. Tokonami, Y. Nakagawa, K. Tomishige, Chem. Commun., 2013, 49, 7034-7036.
[19] G. Bottari, A.J. Kumalaputri, K.K. Krawczyk, B.L. Feringa, H.J. Heeres, K. Barta, ChemSusChem, 2015, 8, 1323-1327.

Journal Pre-proofs

[20] Y. Feng, G. Yan, T. Wang, W. Jia, X. Zeng, J. Sperry, Y. Sun, X. Tang, T. Lei, L. Lin, Green Chem, 2019, 21, 4319-4323.
[21] B. Chen, F. Li, Z. Huang, G. Yuan, Appl. Catal., B, 2017, 200, 192-199.
[22] L. Jiang, P. Zhou, C. Liao, Z. Zhang, S. Jin, ChemSusChem, 2018, 11, 959-964.
[23] C.H. Hao, X.N. Guo, Y.T. Pan, S. Chen, Z.F. Jiao, H. Yang, X.Y. Guo, J. Am. Chem. Soc., 2016, 138, 9361-9364.
[24] M. Delgado-Rebollo, D. Canseco-Gonzalez, M. Hollering, H. Mueller-Bunz, M. Albrecht, Dalton Trans., 2014, 43, 4462-4473.
[25] T. Wang, J. Zhang, W. Xie, Y. Tang, D. Guo, Y. Ni, Catalysts, 2017, 7, 92.
[26] R. Guo, C. Elpelt, X. Chen, D. Song, R.H. Morris, Chem. Commun., 2005, 3050-3052.
[27] M.J. Gilkey, P. Panagiotopoulou, A.V. Mironenko, G.R. Jenness, D.G. Vlachos, B. Xu, ACS Catal., 2015, 5, 3988-3994.
[28] R.M. Bullock, Science, 2013, 342, 1054-1055.
[29] J.F. Sonnenberg, N. Coombs, P.A. Dube, R.H. Morris, J. Am. Chem. Soc., 2012, 134, 5893-5899.
[30] J. Li, J.l. Liu, H.j. Zhou, Y. Fu, ChemSusChem, 2016, 9, 1339-1347.
[31] C. Sui‐Seng, F. Freutel, A.J. Lough, R.H. Morris, Angew. Chem. Int. Ed., 2008, 47, 940-943.
[32] G.H. Wang, X. Deng, D. Gu, K. Chen, H. Tüysüz, B. Spliethoff, H.J. Bongard, C. Weidenthaler, W. Schmidt, F. Schüth, Angew. Chem. Int. Ed., 2016, 55, 11101-11105.
[33] J. Long, Y. Zhou, Y. Li, Chem. Commun., 2015, 51, 2331-2334.
[34] L.J. Malobela, J. Heveling, W.G. Augustyn, L.M. Cele, Ind. Eng. Chem. Res., 2014, 53, 13910-13919.
[35] H. Chen, H. Ruan, X. Lu, J. Fu, T. Langrish, X. Lu, Mol. Catal., 2018, 445, 94-101.
[36] C. Aellig, F. Jenny, D. Scholz, P. Wolf, I. Giovinazzo, F. Kollhoff, I. Hermans, Catal. Sci. Technol., 2014, 4, 2326-2331.
[37] S. Elangovan, C. Topf, S. Fischer, H. Jiao, A. Spannenberg, W. Baumann, R. Ludwig, K. Junge, M. Beller, J. Am. Chem. Soc., 2016, 138, 8809-8814.
[38] A. Bruneau-Voisine, D. Wang, V. Dorcet, T. Roisnel, C. Darcel, J.-B. Sortais, Org. Lett., 2017, 19, 3656-3659.
[39] S. Zhou, G. Chen, X. Feng, M. Wang, T. Song, D. Liu, F. Lu, H. Qi, Green Chem., 2018, 20, 3593-3603.
[40] M. Segall, P.J. Lindan, M.a. Probert, C.J. Pickard, P.J. Hasnip, S. Clark, M. Payne, J. Phys. Condens. Matter, 2002, 14, 2717.
[41] J.P. Perdew, K. Burke, M. Ernzerhof, Phys. Rev. Lett., 1996, 77, 3865.
[42] S. Grimme, J. Antony, S. Ehrlich, H. Krieg, J. Chem. Phys., 2010, 132, 154104.
[43] D. Vanderbilt, Phys. Rev. B, 1990, 41, 7892.
[44] H. Su, K.X. Zhang, B. Zhang, H.H. Wang, Q.Y. Yu, X.H. Li, M. Antonietti, J.S. Chen, J. Am. Chem. Soc., 2017, 139, 811-818.
[45] X.H. Li, S. Kurasch, U. Kaiser, M. Antonietti, Angew. Chem. Int. Ed., 2012, 51, 9689-9692.
[46] M. Zhang, Q. Dai, H. Zheng, M. Chen, L. Dai, Adv. Mater., 2018, 30, 1705431.
[47] Y. Feng, W. Jia, G. Yan, X. Zeng, J. Sperry, B. Xu, Y. Sun, X. Tang, T. Lei, L. Lin, J. Catal., 2020, 381, 570-578.
[48] G. Zhu, L. Wang, H. Lin, L. Ma, P. Zhao, Y. Hu, T. Chen, R. Chen, Y. Wang, Z. Tie, J. Liu, Z. Jin, Adv. Funct. Mater., 2018, 28, 1800003.

Journal Pre-proofs

[49] C. Yang, Q. Gao, W. Tian, Y. Tan, T. Zhang, K. Yang, L. Zhu, J. Mater. Chem. A, 2014, 2, 19975-19982.
[50] L. Qie, W. Chen, H. Xu, X. Xiong, Y. Jiang, F. Zou, X. Hu, Y. Xin, Z. Zhang, Y.J.E. Huang, E. Science, 2013, 6, 2497-2504.
[51] Q. Gan, H. He, K. Zhao, Z. He, S. Liu, Electrochim. Acta, 2018, 266, 254-262.
[52] Y. Fu, Q. Wei, G. Zhang, X. Wang, J. Zhang, Y. Hu, D. Wang, L. Zuin, T. Zhou, Y. Wu, S. Sun, Adv. Energy Mater., 2018, 8, 1801445.
[53] P. Blonski, J. Tucek, Z. Sofer, V. Mazanek, M. Petr, M. Pumera, M. Otyepka, R. Zboril, J. Am. Chem. Soc., 2017, 139, 3171-3180.
[54] G. Wu, K.L. More, C.M. Johnston, P. Zelenay, Science, 2011, 332, 443-447.
[55] Z.S. Wu, A. Winter, L. Chen, Y. Sun, A. Turchanin, X. Feng, K. Müllen, Adv. Mater., 2012, 24, 5130-5135.
[56] M. Yang, Y. Zhong, X. Zhou, J. Ren, L. Su, J. Wei, Z. Zhou, J. Mater. Chem. A, 2014, 2, 12519.
[57] Y. Cao, S. Mao, M. Li, Y. Chen, Y.J.A.C. Wang, 2017, 7, 8090-8112.
[58] D. Deng, L. Yu, X. Chen, G. Wang, L. Jin, X. Pan, J. Deng, G. Sun, X. Bao, Angew. Chem. Int. Ed., 2013, 52, 371-375.
[59] J. Wang, K. Li, H.X. Zhong, D. Xu, Z.L. Wang, Z. Jiang, Z.J. Wu, X.B. Zhang, Angew. Chem., 2015, 54, 10530-10534.
[60] Y.X. Liu, H.H. Wang, T.J. Zhao, B. Zhang, H. Su, Z.H. Xue, X.H. Li, J.S. Chen, J. Am. Chem. Soc., 2019, 141, 38-41.

Journal Pre-proofs

Declaration of interests

☒ The authors declare that they have no known competing financial interests or personal relationships that could have appeared to influence the work reported in this paper.

☒The authors declare the following financial interests/personal relationships which may be considered as potential competing interests:

No conflict of interest exits

Journal Pre-proofs

Graphical Abstract

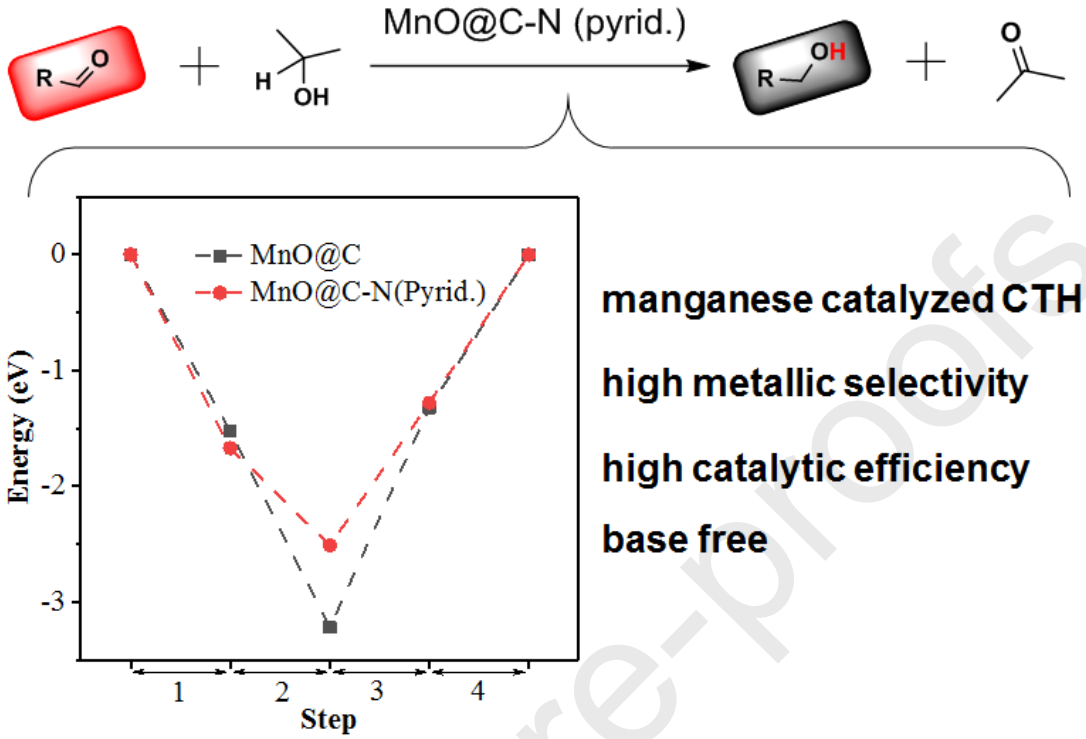

Journal Pre-proofs

Highlights

1. MnO@C-N catalysts have been prepared, characterized and used for CTH for the first time.
2. The role of MnO and N-doping are demonstrated to be responsible for the high selectivity and high conversion, respectively.
3. N-doping can strengthen both basic and acidic sites and reduce the energy barrier

Journal Pre-proofs